Multi-scale x-ray computed tomography analysis of coal microstructure and permeability changes as a function of effective stress

Yihuai Zhang [1*], Xiaomeng Xu [2], Maxim Lebedev [3], Mohammad Sarmadivaleh [1], Ahmed Barifcani [1], Stefan Iglauer [1]

[1]*Department of Petroleum Engineering, Curtin University, 26 Dick Perry Avenue, 6151 Kensington, Australia*

[2]*Faculty of Resources and Safety Engineering, China University of Mining and Technology, Beijing, 100083, China*

[3]*Department of Exploration Geophysics, Curtin University, 26 Dick Perry Avenue, 6151 Kensington, Australia*

[*]corresponding author (yihuai.zhang@postgrad.curtin.edu.au)

Abstract

Gas permeability (k) and porosity (φ) are the most important parameters in CBM/ECBM and CCS in deep unmineable coal seams. k and φ depend on the coal micro structure, and k and φ significantly change with varying effective stress. However, how the coal micro structure is related to such permeability and porosity changes is only poorly understood. We thus imaged sub-bituminous coal samples at two resolutions (medium - 33.7 μm and high - 3.43 μm voxel size) in 3D with an x-ray micro-computed tomograph as a function of applied effective stress; and investigated how

cleat morphology, k and φ are influenced by the changes in effective stress and how these parameters are interrelated. In the images, three phases were identified: micro cleats (void), a mineral phase (carbonate) and the coal matrix. When effective stress increased, the cleats became narrow and closed or disconnected. This resulted in a dramatic permeability drop with increasing effective stress, while porosity decreased only linearly.

Keywords

coal bed methane, effective stress, microCT, microstructure, permeability drop

1. Introduction

Gas permeability is a key factor in coal bed methane (CBM) and enhanced coal bed methane recovery (ECBM), and carbon geo-sequestration in deep unmineable coal seams (Pekot and Reeves, 2002; Moore, 2012). It is well established that gas permeability is highly sensitive to effective stress (Harpalani and Chen, 1992; Palmer and Mansoori, 1996; Karacan and Okandan, 2000; Connell et al., 2010; Cai et al., 2014). This is directly relevant for field production processes, e.g. in ECBM another gas (e.g. nitrogen) is frequently injected to increase the reservoir pore pressure (and thus reduce effective stress) to release methane; or during CBM production reservoir pressure is depleted and effective stress increases. In this context it has been shown that permeability increases by matrix shrinkage due to methane desorption, or permeability decreases by cleat compaction due to pore pressure loss (Harpalani and Chen, 1997; Kumar et al., 2012). It also has been well documented that

permeability decreases drastically with depth (because the overburden stress and thus effective stress increase), and it has been suggested that this is caused by fracture closure (Enever et al., 1999). However, most investigations on coal permeability change focus on the coal swelling effect during gas injection (e.g. CO_2: e.g. Reeves, 2004; Larsen, 2004; Siriwardane et al., 2009) or water encroachment (e.g. Zhang et al., 2016; Stevens et al. 2004); while the influence of effective stress on permeability and associated coal micro structural changes are still poorly understood.

Traditionally dual coal porosity and permeability sets are distinguished, one for the coal matrix and the second set for the natural fracture (cleats) network. The permeability of the coal matrix is much lower than that of the cleats network, thus the cleats network effectively controls the overall permeability of the coal seam (Harpalani and Chen, 1992; Karacan and Okandan, 2000; Connell et al., 2010). Furthermore cleats can be subdivided into butt cleats, which are orthogonal to the coal bedding, and face cleats, which are perpendicular to the coal bedding (Laubach et al., 1998). Cleat properties such as size, structure, orientation and connectivity all significantly affect permeability (Laubach et al., 1998; Flores, 2013). It has been thought that the cleats change when the in-situ stresses change (Chen et al., 2011). However, the variation of the microstructural morphology associated with such changes, especially in micro cleats (less than 20 µm), which are common in the coal matrix (Gamson et al., 1993), is only poorly understood.

Typically such micro-scale investigations are performed via SEM measurements (e.g. Huggins et al., 1980; Kutchko et al., 2013; Ye et al., 2013), and these give a very high resolution (up to 1-20 nm voxel size); however no effective stress can be applied during such a measurement and only 2D images at vacuum conditions can be obtained. The 3D pore morphology, however, is of key importance as it determines the permeability (2D is insufficient information, Stauffer 1979). However, recent developments in the area of x-ray

micro-computed tomography (microCT) applied in core analysis (e.g. Iglauer et al., 2011; Lebedev et al., 2014; Rahman et al., 2016) enable the application of effective stresses to a sample while it is imaged in-situ in 3D at high resolution.

We thus microCT imaged the coal micro structures and their changes in 3D at high resolution as a function of effective stress in-situ and related these changes to independent gas permeability and porosity measurements.

2. Methodology

2.1. Materials

A coal block was acquired from a famous coal mine in the middle of China: the Pingdingshan coal mine, Henan Province. This coal block was identified as sub-bituminous with a fixed carbon content of 54% (±2%) and volatile matter content of 36% (±1%) measured by Chinese Standard GB/T 212-2008 and DL/T 1030-2006; additional properties of this coal are tabulated in Table 1. We specifically selected this coal, because at such low carbon content (less than 75%) always a significant cleat system prevails (Clarkson and Bustin, 1999), which is advantageous when studying the influence of effective stress on cleat morphology and associated changes in permeability. Standard cylindrical (38.1 mm diameter and 76 mm length) core plugs were drilled out of the coal block parallel to the coal bed direction; these plugs were subjected to microCT scanning (Xradia VersaXRM instrument) and gas (N_2) permeability tests in an AP 608 instrument. Furthermore, smaller cylindrical coal plug (5 mm diameter and 10 mm length) were cut from the same coal block adjacent to a position from which the larger plugs were drilled. These smaller plugs were also microCT imaged, but at a much higher resolution, see below.

Furthermore, SEM-EDS tests were performed on more than 10 samples cut from the same coal block, and cleats, coal matrix and a mineral phase were clearly identified, Figure.1. The micro cleats can be divided into three groups according to their spatial position; cleats in the coal matrix (e.g. Figure 1A), cleats between coal matrix and mineral phase (e.g. Figure 1B), and cleats in the mineral phase (e.g. Figure 1D). The mineral phase was identified as calcium carbonate via EDS analysis; these carbonates also filled in some cleats (e.g. Figure 1C).

Table 1: Physical properties of the coal studied.

ρ (g/cm^3)	M_{ad} (%)	V_{daf} (%)	A_{ad} (%)	C_f (%)	E (GPa)	υ
1.35 (±0.03)	6.90 (±0.50)	36.00 (±1.00)	4.20 (±0.20)	54.00 (±2.00)	2.60 (±0.40)	0.31 (±0.1)

Note: ρ is the bulk density; M_{ad} is the moisture content; V_{daf} is the volatile matter; A_{ad} is the ash yield; C_f is the fixed carbon content; E is Young's Modulus; and υ is Poission's ratio. All properties were measured using Chinese Standard GB/T 212-2008.

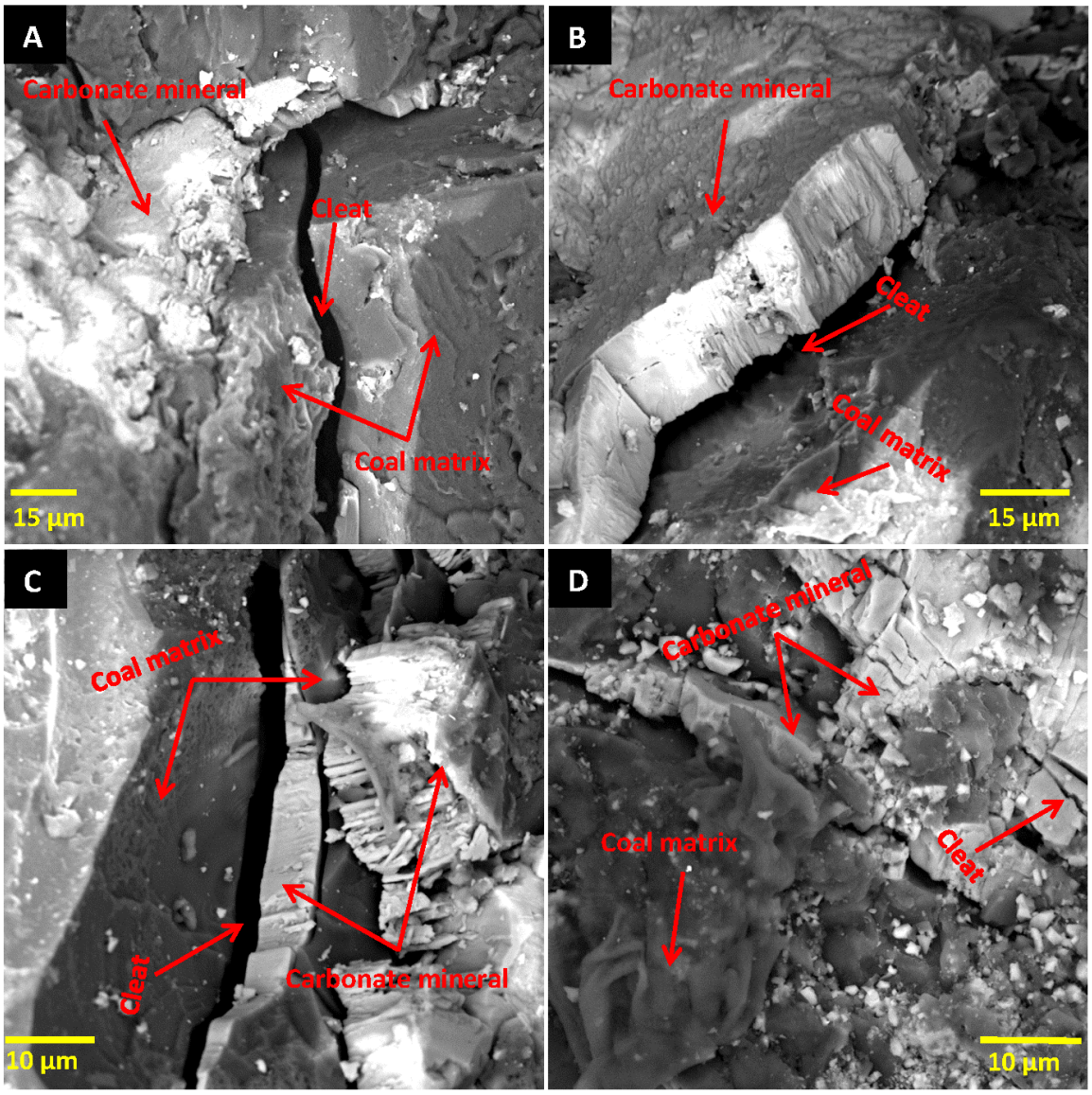

Figure 1. SEM images of the coal sample's surface, where the coal matrix, mineral phase and cleats were clearly identified. (A) cleat inside the coal matrix; (B) cleat between the coal matrix and the mineral phase; (C) minerals filled in the cleat (D) cleat inside the mineral phase.

2.2. Gas permeability measurements

We selected nitrogen for our gas permeability tests (conducted with an AP-608 automated porosimeter-permeameter, accuracy ± 0.1 %) in order to minimize swelling (note that nitrogen causes only a minimal swelling effect: volume strain and linear strain ratio is ≤ 0.2 %, George and Barakat, 2001) and guarantee a minimum degree of gas slippage (Wang et al., 2014). The pore pressure was set constant at 1.38 MPa during the test, while the confining pressure was stepwise increased from 3.5 MPa to 24 MPa. Thus effective stresses from 1.12 - 22.62 MPa were investigated. Four coal plugs (38 mm diameter and 76 mm length, marked as A, B, C, and D) underwent this gas permeability test matrix.

2.3. Micro-CT in-situ imaging

An in-situ micro-CT scanning apparatus was set up (Figure 2), where two different X-ray transparent core holders can be used and different plug sizes imaged (5 mm diameter plugs, "small plugs", cp. Iglauer et al., 2011; Rahman et al., 2016; or 38 mm diameter plugs, "large plugs", Lebedev et al., 2014). A high precision syringe pump (Teledyne ISCO 500D) provided the confining pressure by compressing DI water. Initially a large coal plug (sample E) was mounted inside the large diameter core holder (c.p. Figure 2 E), and the plug was imaged in-situ at three different effective stresses (0 MPa, 5 MPa and 10 MPa) at $(33.7\ \mu m)^3$ 3D voxel resolution at ambient conditions (atmospheric pressure and 296 K). Subsequently a small coal plug was imaged in-situ at the same three effective stresses (0 MPa, 5 MPa and 10 MPa), but now at a much higher resolution, $(3.43\ \mu m)^3$ voxel size. No fluids were injected, i.e. the confining pressures equalled the effective stresses. The x-ray beam diameter was approximately 0.3 μm, and a 1000 x 1000 pixel detector was used for radiograph acquisition. The X-ray accelerating voltage was chosen as 60 kV, and the total acquisition time for one

3D image was approximately 4 hours. The acquired microCT images were then filtered with a 3D non local means filter (Buades et al., 2005) and segmented with a watershed algorithm (Schlüter et al., 2014) for quantitative analysis using Avizo 9 software, cp. Mathews et al., 2011; Jing et al., 2016; Zhang et al., 2016.

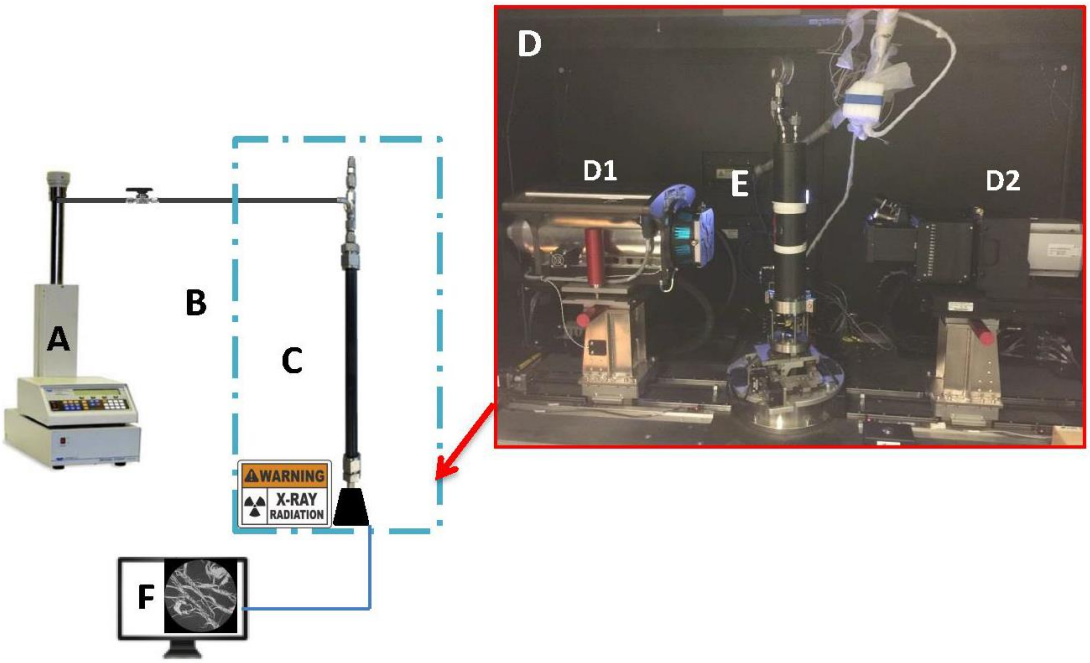

Figure 2. Experimental microCT coreflooding apparatus, (A) confining pressure pump, (B) microCT, (C) core holder for small plug sample (plug diameter = 5 mm), (D) microCT inside view, D1 is the X-ray source, D2 is the X-ray detector, (E) is the core holder for large plug samples (plug diameter = 38 mm), (F) images output and processing.

3. Results and Discussion

3.1. Gas permeability and porosity

Gas permeability (k) and porosity (φ) decreased with increasing effective stress (σ) as expected, Figures 3 and 4. The permeability data followed a power law relation $k = a\sigma^b$, k dropped rapidly when effective stress increased (Figure 3), consistent with earlier

investigations (e.g. Chen et al., 2011; Li et al., 2014). However, the porosity decreased only linearly when effective stress increased, Figure 4. We conclude that any incremental change in effective stress in the high effective stress region does not significantly change permeability, while porosity is still significantly affected.

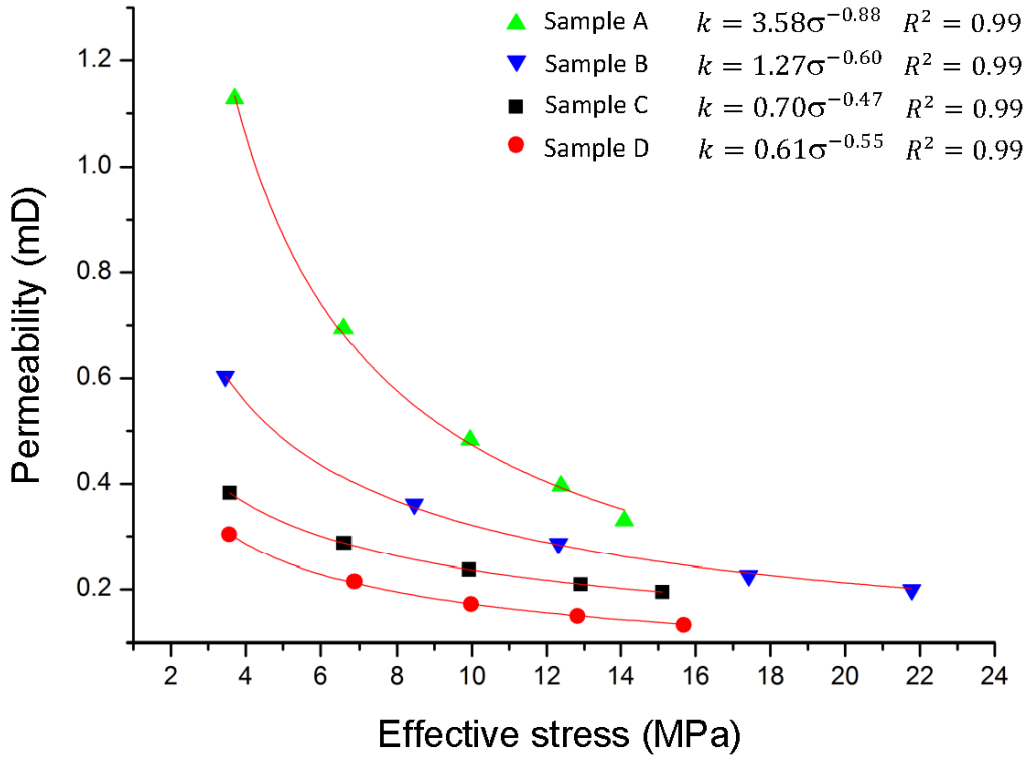

Figure 3. Gas permeability versus effective stress for all four coal plugs tested. The fitting equations are shown in the legend together with their Regression Coefficients.

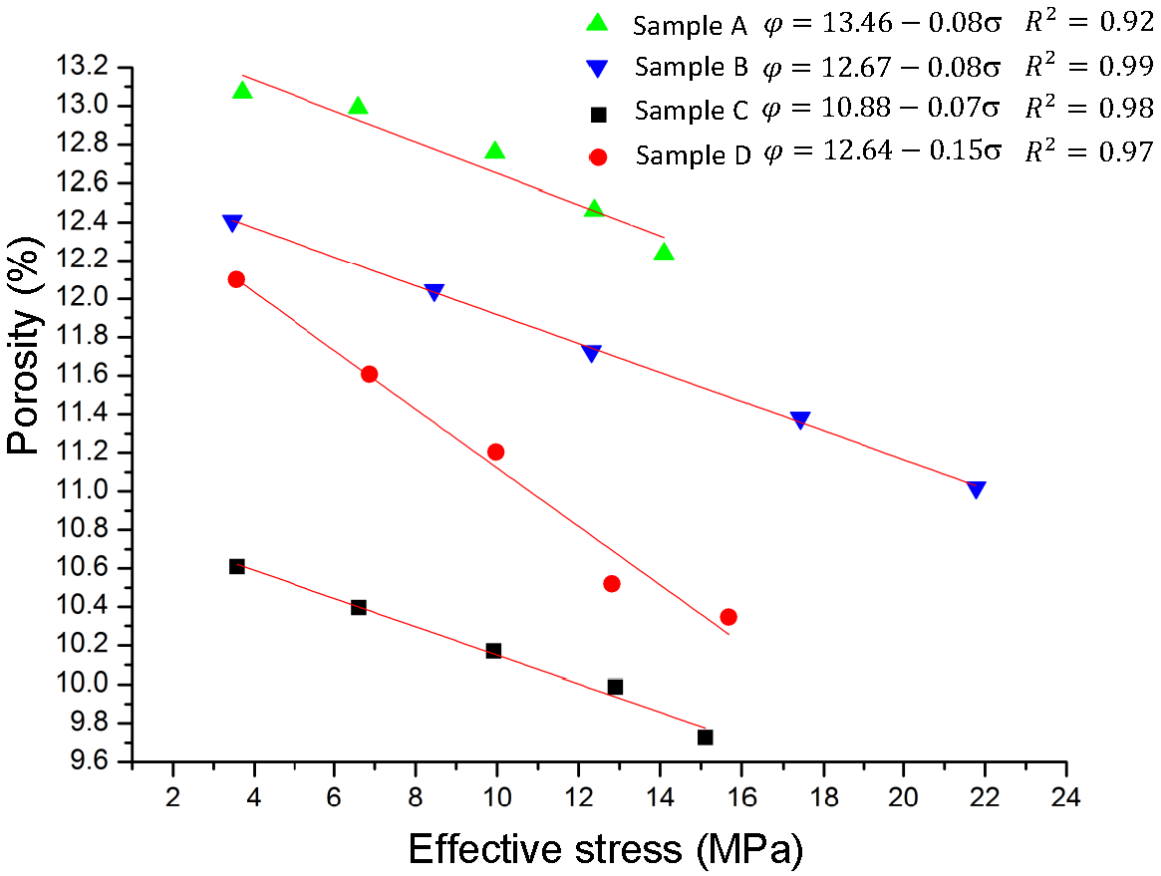

Figure 4. Porosity versus effective stress for the four coal plugs tested. The fitting equations are shown in the legend together with their Regression Coefficients.

3.2. X-ray micro-computed tomography imaging

3.2.1 Qualitative analysis

In the tomograms three phases were identified in the coal plugs (Figure 5): cleats (black), mineral phase (white) and the coal matrix (grey), consistent with previous microCT images of coal (Yao et al., 2009; Golab et al., 2013; Ramandi et al., 2016; Zhang et al., 2016). A few macro cleats were visible in the large plug which was imaged at medium nominal resolution (33.7 μm)^3, Figure 5 A. The macro cleats/fractures were oriented parallel to the mineral veins (Figure 6). The macro cleats at 0 MPa effective stress had a 0.1-0.2 mm width, ~ 1 cm

length, and ~ 1.5 cm depth, Figure 7, and the macro cleat/fracture volume fraction amounted to ~ 0.5 %; these macro cleats/fractures were almost closed at 5 MPa effective stress and completely closed at 10 MPa effective stress, Figure 7. This result thus experimentally confirms the previous hypothesis (McKee et al., 1987; Palmer and Mansoori, 1996; Chen et al., 2011) that cleats close at high effective stress and dramatically reduce coal permeability.

The minerals were also mainly oriented perpendicular to the coal bed, but they showed a stream-like pattern where some mineral streams were connected by perpendicular smaller mineral sub-streams in a ladder-like pattern, "T-junctions". These mineral structures thus somewhat resembled the morphology of "face cleats" and "butt cleats"; this is an indication that mineral invaded and filled the macro cleats after the coal seam formed (Karacan and Okandan, 2000; Su et al., 2001; Solano-Acosta et al., 2007). The structural pattern of the mineral phase, and that it is oriented perpendicular to the coal seam bed, is visualized in Figure 6 in 3D. Furthermore, at high resolution, the mineral veins also reveal subtle structural patterns which were not evident at the medium resolution (Figure 5). In addition, when we zoomed in further, micro cleats were visible (Figure 5 B); these micro cleats/fractures were randomly distributed in the coal matrix with width ~ 5-10 µm and lengths up to 2 mm. Moreover, light grey tones indicating less x-ray dense mineral are present in the image s (Figure 5). This is probably less consolidated calcite (which has nanoporosity which is below the resolution of the microCT images).

When comparing the high resolution images for the three different effective stresses (Figure 8) the change in cleat morphology becomes obvious: the micro cleats in the coal matrix became narrower when effective stress increased (e.g. points 1, 2, and 5 in Figure 8), and some of these micro cleats disconnected from each other creating dead ends for flow (e.g.

point 7 in Figure 8). Moreover, the micro cleats between the matrix and mineral phase disappeared at high effective stress (e.g. points 3 and 4 in Figure 8); however, the micro cleats inside the mineral phase underwent almost no change (e.g. point 6 in Figure 8) because the mineral compressibility is significantly lower than that of the coal matrix.

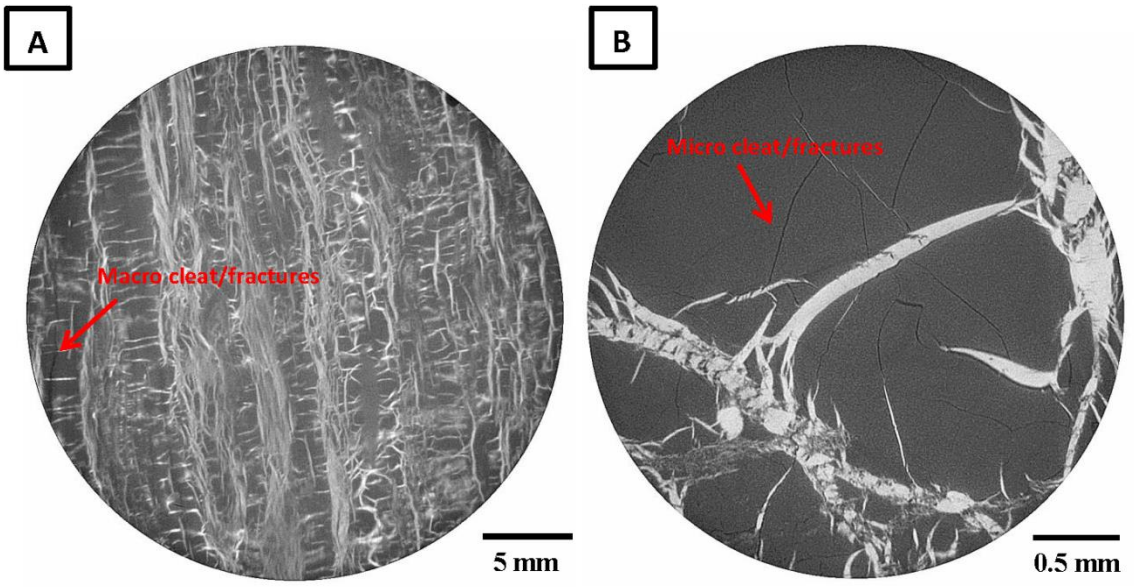

Figure 5. 2D slices through the coal microCT images (0 MPa confining pressure), (A) the large coal plug (33.7 μm nominal resolution); (B) the small coal plug (3.43 μm nominal resolution). Minerals are white, coal matrix is grey and cleats are black.

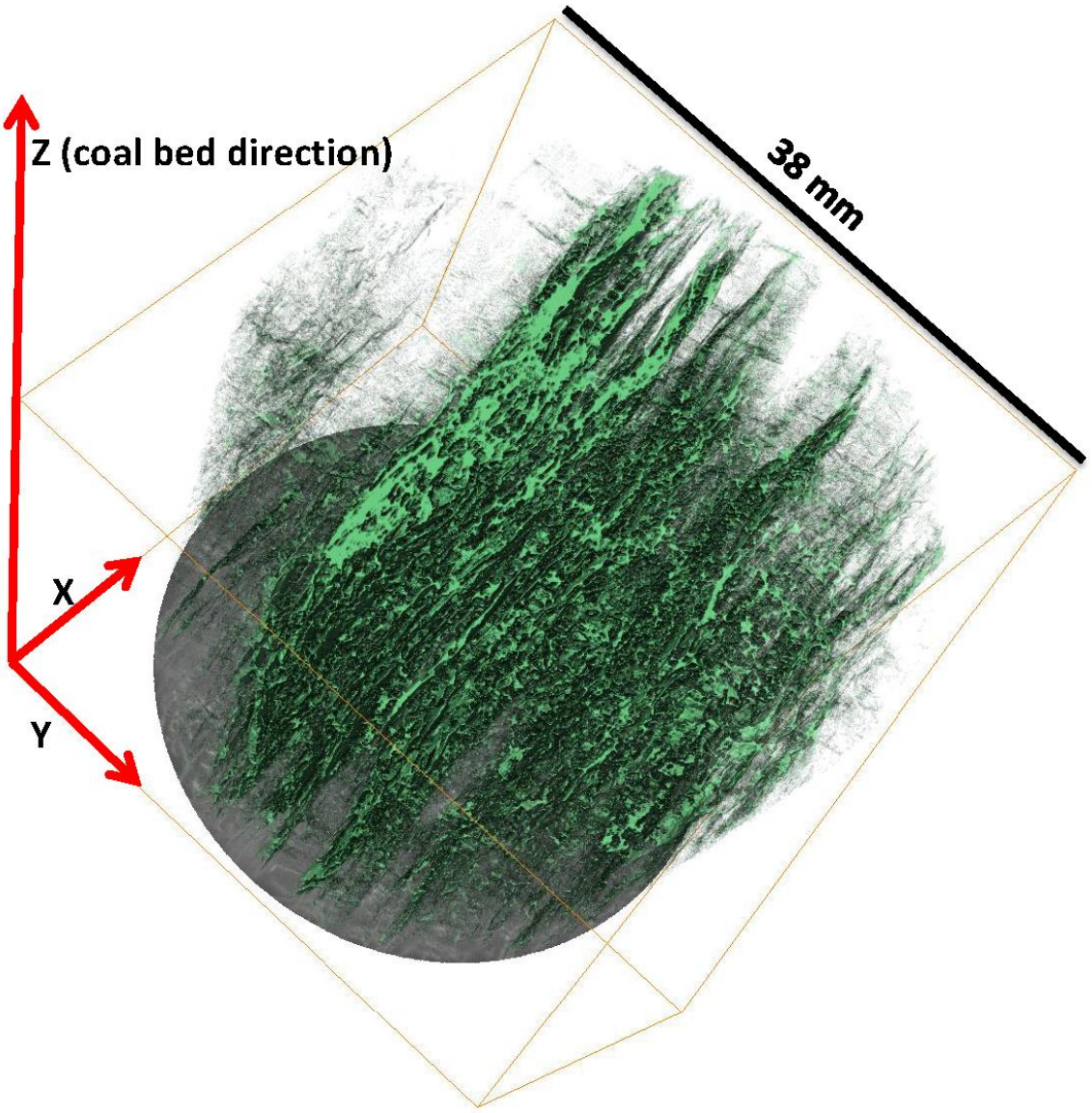

Figure 6. 3D visualization of the mineral phase (green) in the large coal plug at 0 MPa effective stress (38 mm diameter, 33.7 μm voxel resolution). The mineral phase is oriented perpendicular to the coal bed direction (z direction).

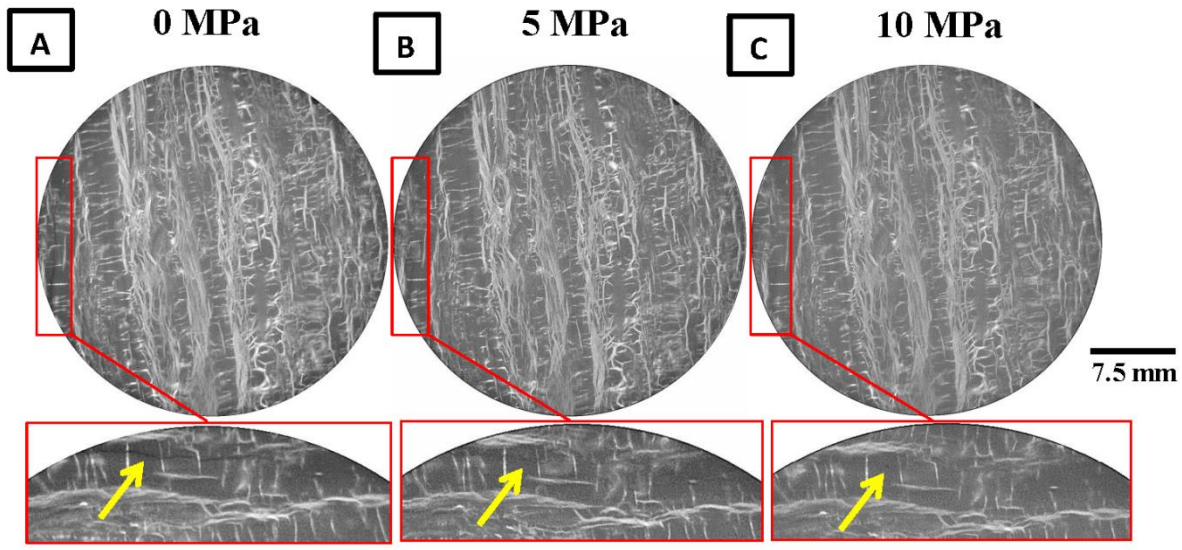

Figure 7. Image slices through the large coal plug (38 mm diameter). Mineral is white, coal matrix grey and cleats are black. Different effective stress situations are illustrated: (A) 0 MPa effective stress, (B) 5 MPa effective stress, and (C) 10 MPa effective stress. The macro cleat observed in (A) (see red boxes and yellow arrows) was almost closed in (B) and completely closed in (C). The mineral phase and coal matrix, however, showed no significant change with increasing effective stress. Nominalresolution is 33.4 µm.

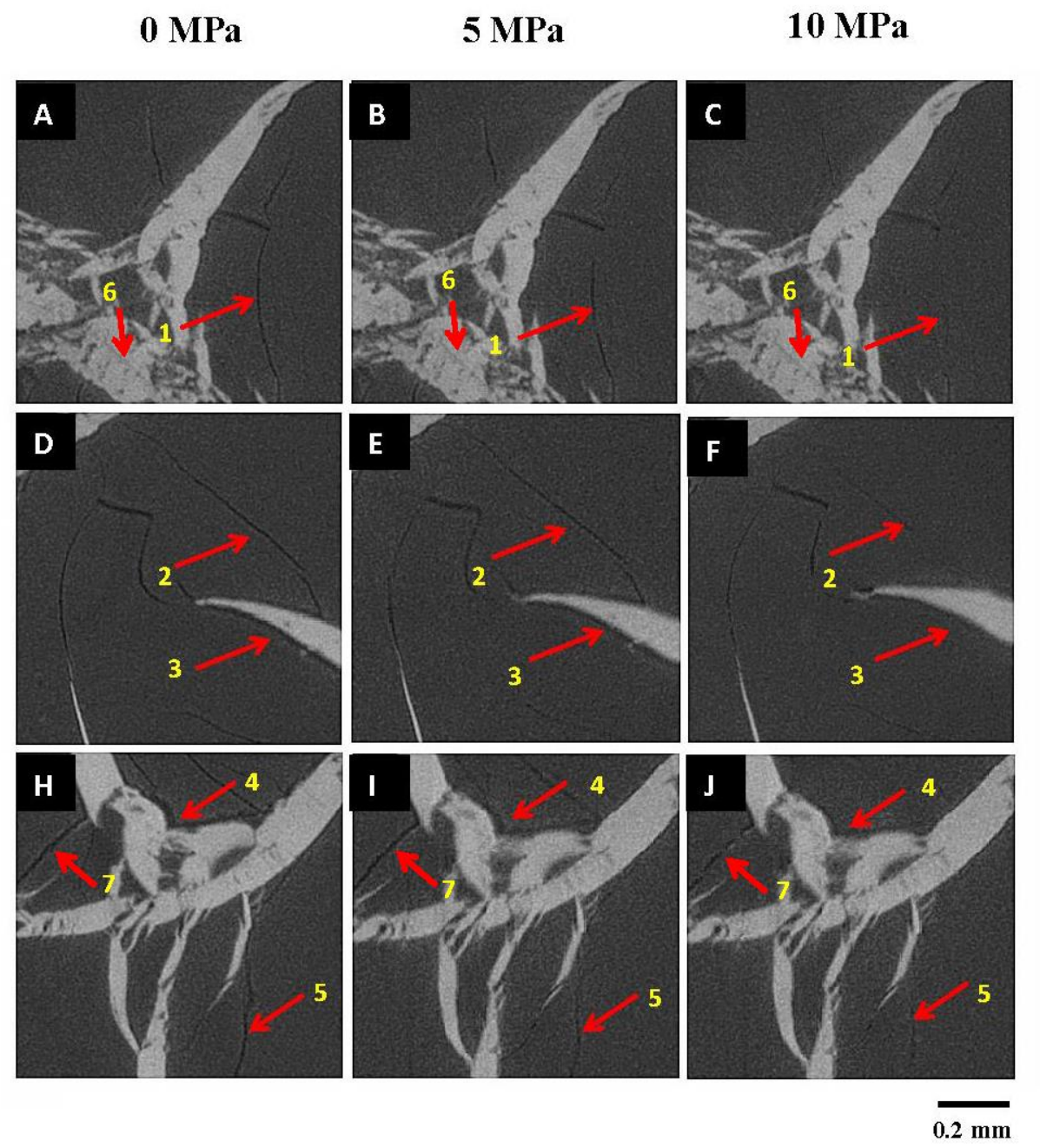

Figure 8. Slices through the coal plug at different effective stresses (0 MPa, 5 MPa and 10MPa), 3.43 μm nominal resolution; A-C, D-F and H-J show three different areas. The numbers and red arrows indicate cleats: cleats 1, 2, 4 and 5 became narrower; cleat 7 became disconnected; cleat 3 disappeared at high effective stress; while cleat 6 showed almost no change.

3.3 Quantitative analysis

The micro cleats porosity (volume of the segmented micro cleats divided by the total volume) as a function of effective stress was quantified on the microCT images, and it significantly decreased with increasing effective stress, by more than half at 10 MPa effective stress. Precisely, cleat porosity decreased from 0.52 %, to 0.33 % and to 0.22 % at 0 MPa, 5 MPa and 10 MPa effective stresses, respectively (Figure 9); however, the volume fractions of the mineral phase and the coal matrix showed no significant difference.

In the segmented images each cleat/fracture was separated and labelled. The cleat size (3D volume, μm^3) distribution was then measured as a function of effective stress (Figure 10). The frequency of the large micro cleats (> 10000 μm^3) decreased dramatically when effective stress increased from 0 MPa to 10 MPa; consistent with the 3D visualizations (Figure 9 A-C) and permeability measurements. However, the frequency of the small micro cleats (< 10000 μm^3) did not change significantly; the number of micro cleats smaller than 100 μm^3 even slightly increased. This could be due to large micro cleats becoming disconnected with increasing effective stress, which are then counted as several small micro cleats, e.g. see Figure 8 J or Figure 9 , where a large micro cleat disconnected at 10 MPa effective stress. Note that cleats propagating outside the imaged volume (i.e. the field of view, FOV) are cropped to the FOV and thus this measurement is biased towards smaller cleats/fractures.

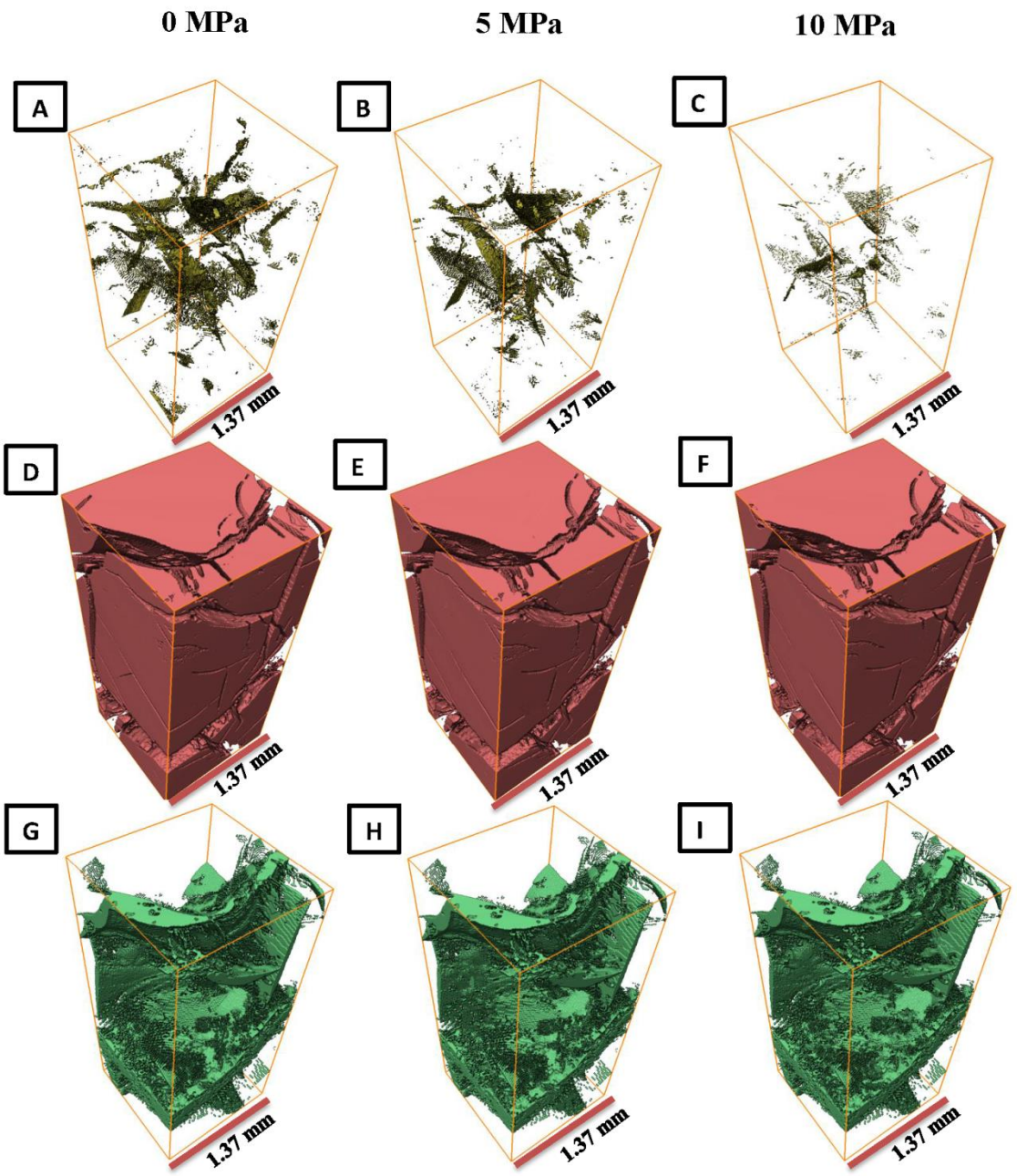

Figure 9. 3D visualizations of the different phases in the small coal plug at the three different effective stresses, 0 MPa, 5MPa and 10MPa (A-C, micro cleats - golden; D-F, coal matrix - red; G-I, mineral phase - green). Volumes shown are 12.2 mm^3 (400 x 400 x 884 voxels) and nominal resolution is 3.43 µm. While the coal matrix and mineral phase show no significant difference, the cleats close upon increasing effective stress.

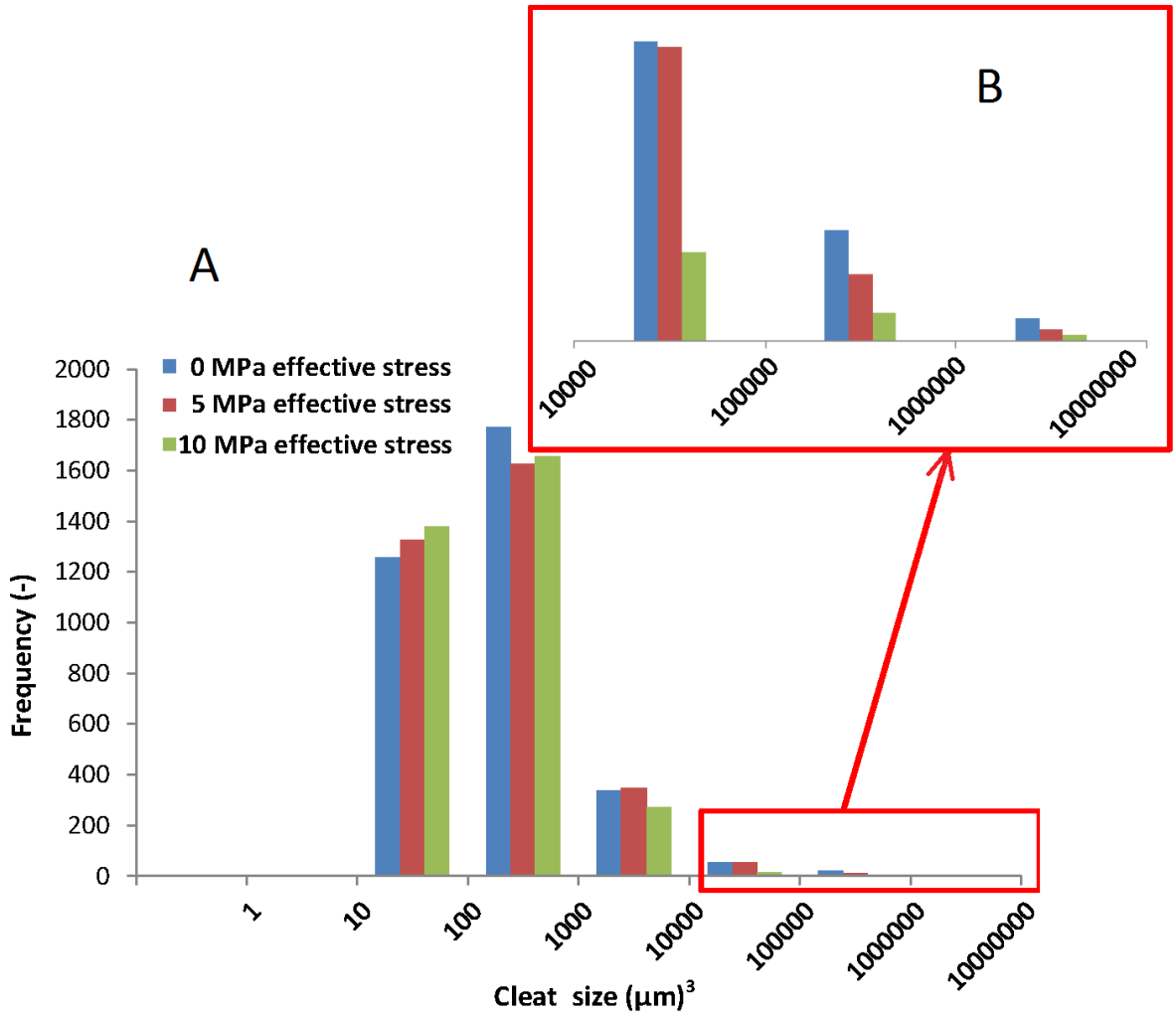

Figure 10. The micro cleat size distribution in the coal as a function of effective stress; (A) full spectrum; (B) zoomed-into the largest cleats area. Large cleat (> 10000 µm^3) frequency dramatically decreased at 10 MPa effective stress.

3.4. Relation between cleat morphology, permeability and porosity

The volume fraction of the cleats measured at the two microCT resolution scales (33.7 µm and 3.43 µm voxel size) was approximately 1.02 % (0.5% macro cleats/fractures + 0.52% micro cleats), which is significantly smaller than the gas porosity (11.5 % ± 0.5 %) measured

on the large plug. We conclude that most void space lies in the coal matrix and is of nanometer scale (i.e. always less than 3 μm, smaller than the highest microCT nominal resolution 3.43 μm), consistent with literature data (Laubach et al., 1998). This is also consistent with the linear porosity decrease with increasing effective stress (Figure 5), i.e. the change in cleat morphology had only a marginal influence on porosity; thus the porosity change is mainly a function of coal compressibility.

Moreover, the underlying mechanism for the rapid permeability drop also becomes clear: as effective stress increases, the cleats close and become disconnected; however, as the cleats are the major fluid conduits (Laubach et al., 1998), permeability drops dramatically, Figure 4, consistent with measurements on larger plugs (Liu and Rutqvist, 2010; Jasinge et al., 2011; Li et al., 2014). The residual permeability at high effective stress (> 10 MPa) is then caused by the remaining cleats in the mineral phase – these cleats are still open as coal matrix compressibility is much higher than the compressibility of the minerals.

4. Conclusions

Porosity and permeability are key properties in CBM/ECBM and CO_2 geo-sequestration applications. However, coal porosity and permeability are functions of the effective stress (Somerton et al., 1975; George and Barakat, 2001; Chen et al., 2011; Jasinge et al., 2011), and the relation between coal micro structure, permeability/porosity and effective stress is only poorly understood. We thus imaged coal plugs at high resolution (33.7 um and 3.43 μm voxel size) with an x-ray micro-computed tomograph in 3D as a function of effective stress (0 MPa, 5 MPa, 10 MPa) to measure the coal micro - structure.

Three phases were identified: cleats (void), coal matrix and mineral phase. Micro cleats closed upon increased effective stress, and the related cleat void space shrank from 0.52 % to 0.22 % when effective stress increased from 0 to 10 MPa. These morphological results are consistent with the gas porosity-permeability tests: gas permeability dropped dramatically (with increasing effective stress), while porosity dropped only linearly.

We conclude that effective stress causes closure of micro cleats in the coal, which leads to a drastic drop in permeability, but only a moderate drop in porosity as most void space is located in the coal matrix as nanopores.

Acknowledgements

The measurements were performed using the μCT system courtesy of the National Geosequestration Laboratory (NGL) of Australia, funded by the Australian Federal Government.

References

Buades, A., Coll, B., Morel, J.-M., 2005. A non-local algorithm for image denoising, Computer Vision and Pattern Recognition, 2005. CVPR 2005. IEEE Computer Society Conference on. IEEE, pp. 60-65.

Cai, Y., Liu, D., Mathews, J.P., Pan, Z., Elsworth, D., Yao, Y., Li, J., Guo, X., 2014. Permeability evolution in fractured coal—Combining triaxial confinement with X-ray computed tomography, acoustic emission and ultrasonic techniques. International Journal of Coal Geology 122, 91-104.

Chen, Z., Pan, Z., Liu, J., Connell, L.D., Elsworth, D., 2011. Effect of the effective stress coefficient and sorption-induced strain on the evolution of coal permeability: experimental observations. International Journal of Greenhouse Gas Control 5, 1284-1293.

Clarkson, C., Bustin, R., 1999. The effect of pore structure and gas pressure upon the transport properties of coal: a laboratory and modeling study. 1. Isotherms and pore volume distributions. Fuel 78, 1333-1344.

Connell, L.D., Lu, M., Pan, Z., 2010. An analytical coal permeability model for tri-axial strain and stress conditions. International Journal of Coal Geology 84, 103-114.

Enever, J., Casey, D., Bocking, M., 1999. The role of in-situ stress in coalbed methane exploration, Coalbed Methane: Scientific, Environmental and Economic Evaluation. Springer, pp. 297-303.

Flores, R.M., 2013. Coal and coalbed gas: fueling the future. Newnes.

Gamson, P.D., Beamish, B.B., Johnson, D.P., 1993. Coal microstructure and micropermeability and their effects on natural gas recovery. Fuel 72, 87-99.

George, J.S., Barakat, M., 2001. The change in effective stress associated with shrinkage from gas desorption in coal. International Journal of Coal Geology 45, 105-113.

Golab, A., Ward, C.R., Permana, A., Lennox, P., Botha, P., 2013. High-resolution three-dimensional imaging of coal using microfocus X-ray computed tomography, with special reference to modes of mineral occurrence. International Journal of Coal Geology 113, 97-108.

Harpalani, S., Chen, G., 1992. Effect of gas production on porosity and permeability of coal, Proceedings of the Symposium of Coalbed Methane R and D in Australia, pp. 67-73.

Harpalani, S., Chen, G., 1997. Influence of gas production induced volumetric strain on permeability of coal. Geotechnical & Geological Engineering 15, 303-325.

Huggins, F., Kosmack, D., Huffman, G., Lee, R., 1980. Coal mineralogies by SEM automatic image analysis. Scanning Electron Microsc.;(United States) 1980.

Iglauer, S., Paluszny, A., Pentland, C.H., Blunt, M.J., 2011. Residual CO2 imaged with X-ray micro-tomography. Geophysical Research Letters 38.

Jasinge, D., Ranjith, P., Choi, S.-K., 2011. Effects of effective stress changes on permeability of latrobe valley brown coal. Fuel 90, 1292-1300.

Jing, Y., Armstrong, R.T., Ramandi, H.L., Mostaghimi, P., 2016. Coal cleat reconstruction using micro-computed tomography imaging. Fuel 181, 286-299.

Karacan, C.Ö., Okandan, E., 2000. Fracture/cleat analysis of coals from Zonguldak Basin (northwestern Turkey) relative to the potential of coalbed methane production. International Journal of Coal Geology 44, 109-125.

Kumar, H., Elsworth, D., Liu, J., Pone, D., Mathews, J.P., 2012. Optimizing enhanced coalbed methane recovery for unhindered production and CO 2 injectivity. International Journal of Greenhouse Gas Control 11, 86-97.

Kutchko, B.G., Goodman, A.L., Rosenbaum, E., Natesakhawat, S., Wagner, K., 2013. Characterization of coal before and after supercritical CO 2 exposure via feature relocation using field-emission scanning electron microscopy. Fuel 107, 777-786.

Larsen, J.W., 2004. The effects of dissolved CO 2 on coal structure and properties. International Journal of Coal Geology 57, 63-70.

Laubach, S., Marrett, R., Olson, J., Scott, A., 1998. Characteristics and origins of coal cleat: a review. International Journal of Coal Geology 35, 175-207.

Lebedev, M., Iglauer, S., Mikhaltsevich, V., 2014. Acoustic Response of Reservoir Sandstones during Injection of Supercritical CO 2. Energy Procedia 63, 4281-4288.

Li, Y., Tang, D., Xu, H., Meng, Y., Li, J., 2014. Experimental research on coal permeability: The roles of effective stress and gas slippage. Journal of Natural Gas Science and Engineering 21, 481-488.

Liu, H.-H., Rutqvist, J., 2010. A new coal-permeability model: internal swelling stress and fracture–matrix interaction. Transport in Porous Media 82, 157-171.

Mathews, J.P., Pone, J.D.N., Mitchell, G.D., Halleck, P., 2011. High-resolution X-ray computed tomography observations of the thermal drying of lump-sized subbituminous coal. Fuel Processing Technology 92, 58-64.

McKee, C.R., Bumb, A.C., Koenig, R.A., 1987. Stress-dependent permeability and porosity of coal, International Coalbed Methane Symposium, University of Alabama, Tuscaloosa, Alabama, pp. 183-193.

Moore, T.A., 2012. Coalbed methane: a review. International Journal of Coal Geology 101, 36-81.
Okabe, H., Blunt, M.J., 2004. Prediction of permeability for porous media reconstructed using multiple-point statistics. Physical Review E 70, 066135.

Palmer, I., Mansoori, J., 1996. How permeability depends on stress and pore pressure in coalbeds: a new model, SPE Annual Technical Conference and Exhibition. Society of Petroleum Engineers.

Pekot, L., Reeves, S., 2002. Modeling coal matrix shrinkage and differential swelling with CO2 injection for enhanced coalbed methane recovery and carbon sequestration applications. Topical report, US Department of Energy.

Rahman, T., Lebedev, M., Barifcani, A., Iglauer, S., 2016. Residual trapping of supercritical CO 2 in oil-wet sandstone. Journal of colloid and interface science 469, 63-68.

Ramandi, H.L., Mostaghimi, P., Armstrong, R.T., Saadatfar, M., Pinczewski, W.V., 2016. Porosity and permeability characterization of coal: a micro-computed tomography study. International Journal of Coal Geology 154, 57-68.

Reeves, S.R., 2004. The Coal-Seq project: Key results from field, laboratory and modeling studies, Proceedings of the 7th International Conference on Greenhouse Gas Control Technologies (GHGT-7). Citeseer, pp. 1399-1406.

Schlüter, S., Sheppard, A., Brown, K., Wildenschild, D., 2014. Image processing of multiphase images obtained via X-ray microtomography: a review. Water Resources Research 50, 3615-3639.

Siriwardane, H., Haljasmaa, I., McLendon, R., Irdi, G., Soong, Y., Bromhal, G., 2009. Influence of carbon dioxide on coal permeability determined by pressure transient methods. International Journal of Coal Geology 77, 109-118.

Solano-Acosta, W., Mastalerz, M., Schimmelmann, A., 2007. Cleats and their relation to geologic lineaments and coalbed methane potential in Pennsylvanian coals in Indiana. International Journal of Coal Geology 72, 187-208.

Somerton, W.H., Söylemezoğlu, I., Dudley, R., 1975. Effect of stress on permeability of coal, International journal of rock mechanics and mining sciences & geomechanics abstracts. Elsevier, pp. 129-145.

Stauffer, D., Scaling theory of percolation clusters, Physics reports, 54, 1-74, 1979.

Stevens, S.H., Spector, D., Riemer, P., Enhanced coalbed methane recovery using CO_2 injection: worldwide resource and CO2 sequestration potential, in: SPE International Oil and Gas Conference and Exhibition in China, Society of Petroleum Engineers, 1998.

Su, X., Feng, Y., Chen, J., Pan, J., 2001. The characteristics and origins of cleat in coal from Western North China. International Journal of Coal Geology 47, 51-62.

Wang, G., Ren, T., Wang, K., Zhou, A., 2014. Improved apparent permeability models of gas flow in coal with Klinkenberg effect. Fuel 128, 53-61.

Yao, Y., Liu, D., Che, Y., Tang, D., Tang, S., Huang, W., 2009. Non-destructive characterization of coal samples from China using microfocus X-ray computed tomography. International Journal of Coal Geology 80, 113-123.

Ye, R., Xiang, C., Lin, J., Peng, Z., Huang, K., Yan, Z., Cook, N.P., Samuel, E.L., Hwang, C.-C., Ruan, G., 2013. Coal as an abundant source of graphene quantum dots. Nature communications 4.

Zhang, Y., Lebedev, M., Sarmadivaleh, M., Barifcani, A., Rahman, T., Iglauer, S., 2016. Swelling effect on coal micro structure and associated permeability reduction. Fuel 182, 568-576.